All-Optical 500-Mb/s UWB Transceiver: An Experimental Demonstration

Mohammad Abtahi, *Member, IEEE*, Mehrdad Mirshafiei, Sophie LaRochelle, *Member, IEEE, OSA*, and Leslie A. Rusch, *Senior Member, IEEE, OSA*

***Abstract*—We propose and demonstrate experimentally, for the first time, a prototype for all-optical ultra-wideband (UWB) transceiver at 500 Mb/s. We report 1) UWB pulse optimization that takes into account the transmitter RF front end and the U.S. Federal Communications Commission (FCC) spectral mask, 2) a new approximate match filter receiver using optical signal processing, and 3) modulation at 500 Mb/s. Our previous optimization of UWB pulse shapes was based only on the FCC spectral mask, without taking into account the frequency response of the RF components (amplifier and antenna) in the UWB transmitter. Here, we modify our pulse optimization technique to ensure that the equivalent isotropic radiated power (EIRP) from the transmitter meets FCC specifications. For the RF hardware used, we achieve 63.6% efficiency over the FCC mask, which yields an 11.6- and a 5.9-dB improvement over Gaussian monocycle and doublet pulses, respectively. We also introduce simple optical signal processing at the receiver that allows the incoming RF signal to be matched against a square pulse whose duration is adapted to the channel. The exact matched filter would require a new optimized pulse that would include not only hardware frequency response but channel effects that vary with antenna placement as well. The proposed approximation allows a simple variation of the pulse duration: an increase to account for pulse expansion in the channel but an upper limit to combat multipath effects. Finally, we demonstrate the optimized pulse and approximate match filter receiver at 500 M/s. We attain a 10^{-6} bit error rate at a 65-cm separation line of sight (LOS) link with simple on-off keying and no forward error correction.**

***Index Terms*—Antenna, BER, EIRP, Fiber Bragg grating, on–off keying (OOK), spectral pulse shaping, ultra-wideband (UWB).**

I. Introduction

ULTRA-WIDEBAND (UWB) radio is considered to be a promising technique for wireless short-range, high-speed data communications, as well as in many other applications in medicine, the military, precision navigation, sensor networks, surveillance, and so on. UWB is attractive not only for the enormous unlicensed frequency band approved by the U.S. Federal Communications Commission (FCC) in 2002 but also because of its potential to support high data rates, high temporal resolution, and penetration through obstacles [1].

Manuscript received February 13, 2008; revised April 18, 2008. Current version published October 10, 2008. This work was supported in part by TELUS Corporation and the Canadian Natural Science and Engineering Research Council.

The authors are with the Center for Optics, Photonics, and Lasers (COPL), Electrical and Computer Engineering Department, Université Laval, Quebec City, QC, G1V0A6 Canada (e-mail: abtahi@gel.ulaval.ca; mehrdad.mirshafiei.1@ulaval.ca; larochel@gel.ulaval.ca; rusch@gel.ulaval.ca).

Color versions of one or more of the figures in this paper are available online at http://ieeexplore.ieee.org.

Digital Object Identifier 10.1109/JLT.2008.925621

The maximum permissible radiated power by the transmit antenna in UWB systems is limited by FCC regulations requiring that the effective isotropically radiated power (EIRP) remains below a specified spectral mask [2]. UWB systems are highly power limited due to this imposed mask, compared to more conventional (narrowband) systems. Pulse-shaping techniques that eke out the greatest legally allowed transmission power are critical to enhancing UWB performance.

Various optical UWB pulse-generation techniques have been proposed [3]–[6]. Most are based on optical spectral shaping and frequency-to-time conversion [4]–[6] using various approaches. The bulk pulse shaping device in [5] is a 4f-grating and lens apparatus with a spatial light modulator (SLM) to modulate the amplitude of frequency components. A reflective approach is used in [6], where the SLM is replaced by a single-layer liquid crystal modulator (LCM). The main advantage of the waveform generators in [5] and [6] is the reprogrammability of pulse-shaping filters (SLM or LCM), which makes it possible to generate arbitrary waveforms. This technique is used in [7] to tailor the UWB power spectrum based on a predefined profile.

Recently, we proposed and experimentally demonstrated an efficient, high-precision technique for optical generation of an FCC-compliant UWB waveform using fiber Bragg gratings (FBG) [8]. The pulse shapes are designed, using methods in [9], to maximize the transmit power while constraining the power spectral density (PSD) of the pulse to respect the FCC mask. In our technique [8], the spectrum of a broadband coherent source (e.g., a mode-locked laser) is flattened and shaped using a chirped grating to attain the optimized time domain pulse shape in the frequency domain. A length of single mode fiber (SMF) is used as a dispersive medium to perform frequency-to-time conversion. The high precision of this technique is because of the removal of the unwanted, positive rectangular pulse (pedestal) superimposed on the desired waveform by employing a two-branch structure and balanced photodetection. The pedestal can be seen in results reported in [4]–[7]. A programmable version of the pulse generator allows tuning to one of these pulses: the monocycle, doublet, or FCC-compliant pulse [10].

Our previous designs did not take into account the frequency response of the transmit antenna. As the FCC mask refers to EIRP, compliance is always dependent on the transmit antenna, and not only on the UWB pulse [11]. In fact, the frequency response of the antenna is often used to compensate for the elevated power level of typical UWB pulse shapes (e.g., monocycle and doublet) at low frequencies. In this paper, we consider the antenna frequency response of a commercially available wideband antenna, and optimize our UWB pulse shape to maximize power

0733-8724/$25.00 © 2008 IEEE

Authorized licensed use limited to: BIBLIOTHEQUE DE L'UNIVERSITE LAVAL. Downloaded on December 3, 2008 at 10:43 from IEEE Xplore. Restrictions apply.

transmitted subject to the FCC mask of the pulse after RF amplification and transmission by the antenna. We are able to achieve 70% exploitation of the power permitted by the FCC mask.

To our knowledge, the highest bit rate achieved to date for UWB transmission over very short LOS links is 890 Mb/s (provided experimentally by Pulse-Link [12]) and is significantly reduced (less than 120 Mb/s) at longer distances. This system consists of a completely electronic transmitter and receiver. Again, to our knowledge, our paper represents the only all-optical UWB system working at 500 Mb/s (short-range, LOS), and we can easily move up to 700 or 800 Mb/s. The only problem we encountered is our non-tunable repetition rate optical coherent source, which is discussed further in Section V-C. This problem disappears when using an optical source with tunable rate, low energy, and low timing jitter.

We also introduce simple optical signal processing at the receiver that allows the incoming RF signal to be matched against a square pulse whose duration is adapted to the channel. The proposed optical receiver exploits time-gating to reject multipath returns. The on-off keying (OOK) modulated incoming signal from a line of sight (LOS) point-to-point link at 500 Mb/s is sent to the RF input of an external modulator whose input is an optical signal with roughly rectangular pulses at the same repetition rate.

An adjustable delay line is used to align the start of the received pulse with that of the local pulse. A low speed photodetector (PD) with a roughly 500-MHz frequency response is then used to collect the energy of the received UWB pulse (which acts as an integrator) and detect the signal (optical-to-electrical conversion).

Our rectangular pulse acts as a rough matched filter, correlating the received signal with a pulse with a similar frequency response. The rectangular pulse is longer than the transmitted pulse to capture energy in a UWB pulse elongated during propagation. The pulse width is selected to truncate the tail of the received pulse containing the multipath reflections. The pulse duration is channel dependent and set by the use of a dispersive medium. Note that optimal match filtering would require adapting the pulse shape at the receiver to the propagation channel—a prohibitively complex procedure. Here, we use one simply parameter, i.e., pulse duration, to achieve a good approximation of the matched filter.

The use of an external modulator at the receiver makes it more complex, but cost could be reduced by the use of photonic integration in an all-optical transceiver structure.

The remainder of this paper is organized as follows. In Section II, a new effective spectral mask is defined, incorporating information on the antenna gain profile. This mask is used in Section III to design the optimum UWB waveform. The structure of the proposed UWB transceiver is explained in Section IV. The experimental results are provided in Section V. Finally, we conclude the paper in Section VI.

II. Effective Spectral Mask

According to FCC regulations, UWB systems must comply with stringent EIRP limits in the frequency band of operation. For a measured peak power density of an antenna under test, EIRP is defined as the amount of power emitted by a hypothetical isotropic antenna that would produce the same peak power density. EIRP is given as [11]

$$\text{EIRP} = P_T(f)G_T(f) \tag{1}$$

where $P_T(f)$ is the transmit power spectral density, and $G_T(f)$ is the transmit antenna gain profile. Note that $P_{ave} = \int_{-\infty}^{+\infty} P_T(f)df$ is the total average power fed to the antenna.

A general procedure for determining the EIRP per unit bandwidth is to use the Friis power transmission formula in its simple form [11]

$$\frac{P_R(f)}{P_T(f)} = G_T(f)G_R(f)\left(\frac{c}{4\pi rf}\right)^2 \tag{2}$$

where $P_R(f)$ is the received power spectral density, $G_R(f)$ is the receive antenna gain profile, c is the speed of light, r is the far-field radial distance between the transmitter and the receiver, and f is the frequency of operation. The antennas are assumed to be both impedance and polarization matched. Equation (2) is valid for r larger than $2d^2/\lambda$, where d is the maximum dimension of the antennas, and λ is the free space wavelength. When d is much greater than the wavelength, the far-field criterion becomes very large, and the field strength that must be measured at the far-field location is less than the receiver noise floor. In such cases, the near-field measurement techniques should be used for EIRP determination [13]. For the antenna dimensions and the maximum frequency of interest (10 GHz) for UWB, the far-field approximation is valid.

To obtain the transmitted EIRP, we use similar antennas at transmitter and receiver. We measure the total frequency response of the transmit-receive pair $G_{CH}(f) = P_R/P_T$ using a network analyzer. The orientations of the antennas are adjusted carefully so that they can see each other from the same angle. As transmit and receive antennas are comparable, we take $G_T(f) = G_R(f)$, and from (1) and (2), we have

$$\text{EIRP} = P_T(f)\sqrt{G_{CH}(f)}\left(\frac{4\pi rf}{c}\right) \tag{3}$$

Furthermore, no multipath reflections are assumed in the Friis formula. We first attenuate the major reflections by placing RF absorbers around the antennas during G_{CH} measurement and then remove the reminding multipath reflections simply by truncating the channel impulse response. The truncated impulse response is then Fourier transformed and used in (3) for EIRP calculation.

As mentioned in the introduction, the UWB pulse shape $x(t)$ should be designed to achieve the maximum permissible power, subject to EIRP being below the FCC mask. Therefore, the pulse design strongly depends on the transmit antenna gain $G_T(f)$. EIRP $\leq S_{FCC}$ leads us to define an effective spectral mask for a given antenna by

$$M(f) = cS_{FCC}(f)/4\pi rf\sqrt{G_{CH}(f)} \tag{4}$$

Authorized licensed use limited to: BIBLIOTHEQUE DE L'UNIVERSITE LAVAL. Downloaded on December 3, 2008 at 10:43 from IEEE Xplore. Restrictions apply.

where $S_{FCC}(f)$ is the FCC mask. Now, the power spectral density of the UWB pulse should respect $M(f)$ instead of the FCC mask. $M(f)$ has singularities at very low frequency (due to $1/f$ dependence) and around the cutoff frequencies of G_{CH}. Thus, we confine our design to frequency band where $M(f)$ is well defined. In the case of the wideband antennas used, the limit frequencies cover the main UWB band between 3.1 to 10.6 GHz.

In the next section, we explain our pulse design technique using an optimization procedure to maximize the total average power under the newly defined mask that is antenna dependent.

III. UWB Pulse Design

Based on the effective spectral mask generated in the previous section, we find optimal waveforms which maximize the transmitted power while conforming to the new mask. In this paper, we follow the optimization procedure proposed in [9] following the new effective spectral mask. The optimal pulse is synthesized using a digital finite impulse response (FIR) filter structure. Gaussian monocycle pulses form the building blocks of the filter. Given a filter with L taps, the optimal pulse $x(t)$ is expressed as

$$x(t) = \sum_{k=o}^{L-1} w[k]\mathrm{g_m}(t - kT_0) \tag{5}$$

where T_0 is the tap spacing, $\{w[k]\}_{k=0}^{k=L-1}$ are the filter tap coefficients to be determined by the optimization process, and $g_m(t) = At\exp(-2(t/\tau)^2)$ is the Gaussian monocycle pulse with pulse duration of about 4τ and A serving as a scaling constant. The Fourier transform of $x(t)$, $X(f)$ can be expressed as $|X(f)| = |W(e^{j2\pi fT_0})||G_m(f)|$, where $G_m(f)$ is the Fourier transform of the Gaussian monocycle, and W is the discrete Fourier transform of vector $\vec{w}$ defined by $\vec{w} = [w[0], w[1], \cdots, w[L-1]]$.

The UWB pulse $x(t)$ should be designed in order to maximize the power within the UWB frequency range F_P

$$\max \int_{F_p} |X(f)|^2 df, \quad f \in F_p. \tag{6}$$

This maximization is subject to the PSD restrictions imposed by the effective spectral mask. As explained in the previous section, EIRP $\leq S_{FCC}(f)$ corresponds to the following condition for the UWB pulse:

$$|X(f)|^2 \leq M(f). \tag{7}$$

Equations (6) and (7) define a non-convex optimization problem, requiring rigorous numerical methods. To transform this into a convex optimization problem, we use the autocorrelation of w, which is defined as $r[k] = \sum_i w[i]w[i+k]$ with vector representation by $\vec{r} = [r[0], r[1], \cdots, r[L-1]]^T$. We define two auxiliary vectors $\vec{v}(f, L)$ and $\vec{u}(f, L)$ by

$$\vec{v}(f, L)_i = e^{j2\pi(i-1)fT_0}, \quad i = 1, \ldots, L$$
$$\vec{u}(f, L)_i = \beta_i \cos(2\pi(i-1)fT_0)$$

where $\beta_1 = 1$, and $\beta_{i\neq 1} = 2$. Using simple calculation, the optimization goal in (6) can be simplified to $\max \vec{b}.\vec{r}$, where $\vec{b} = \int_{F_P} \vec{u}(f, L)|G_m(f)|^2 df$.

The FCC-imposed limit on EIRP can be now expressed as $|W(e^{j2\pi fT_0})|^2|G_m(f)|^2 \leq M(f)$. Therefore, the optimization is

$$\begin{aligned} &\max\{\vec{b}.\vec{r}\} \\ &\text{subject to : } \vec{u}(f, L)\vec{r} \leq M(f)/\left|G_m(f)\right|^2, \quad f \in F_P \end{aligned} \tag{8}$$

To ensure a valid autocorrelation vector, we also require

$$\vec{u}(f, L)\vec{r} \geq 0 \quad f \in F_P. \tag{9}$$

These constraints, which form a convex semi-infinite linear optimization problem, can be discretized to form a finite linear program. While this gives an approximate solution, enough samples ensure acceptable precision of the solution. The problem can be solved using a convex cone optimization program, such as the Matlab SeDuMi optimization tool [14].

First, we transform our optimization problem (8) to the SeDuMi format (see the Appendix) to obtain the tap coefficients. Once we know the optimal tap coefficients, finding the UWB pulse which optimally exploits and respects the effective spectral mask is trivial via (5). The greater the number of taps, the better the fit of the mask.

IV. UWB Transceiver Structure

A. Pulse Shaping and Transmitter Structure

The details of our pulse shaping technique, as well as a theoretical analysis, are provided in [8]. We use the same pulse generation setup, although now, the FBG responsible for the spectral pulse shaping follows our new design. The complete setup of the transceiver is shown in Fig. 1, where a passive mode-locked fiber laser (MLFL) with large full-width at half-maximum (FWHM) bandwidth is used as a coherent broadband source. The spectrum of the laser is first flattened over the desired bandwidth by an appropriately designed FBG. Then a pulse-shaping filter modifies the spectrum to achieve the desired time-domain pulse. The spectrally shaped pulse is sent to a dispersive medium (e.g., SMF) to perform frequency-to-time mapping.

We use a pulse-shaping grating whose complex apodization profile is optimized to imprint the desired pulse shape on the spectrum of the source. The generated pulse is the summation of the desired pulse shape and a rectangular pulse with the same width. The unwanted additive rectangular pulse superimposed on the desired pulse shape changes the spectrum of the signal in all frequencies with strong, unwanted spectral components at

Authorized licensed use limited to: BIBLIOTHEQUE DE L'UNIVERSITE LAVAL. Downloaded on December 3, 2008 at 10:43 from IEEE Xplore. Restrictions apply.

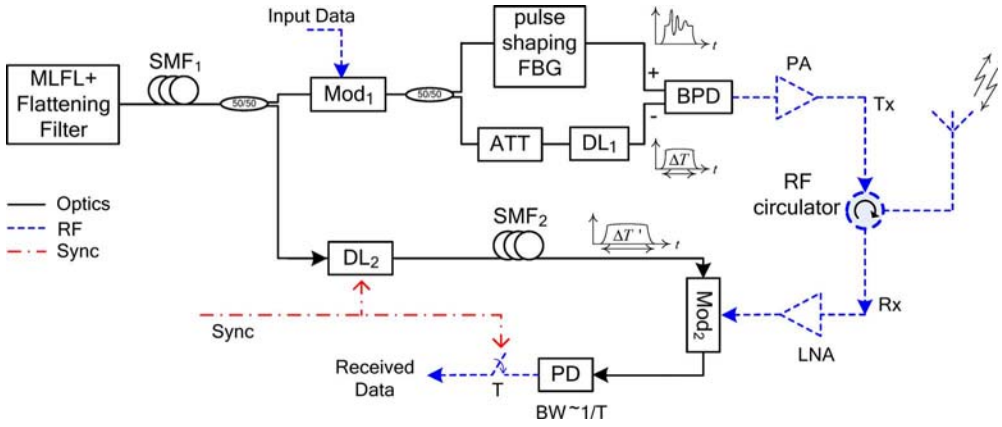

Fig. 1. Schematic diagram of the all-optical UWB transceiver.

low frequencies ($<\sim$1 GHz). To remove the rectangular pulse, the optical signal is divided into two arms, and in the second arm, an optical delay line (DL_1) and a variable attenuator (ATT) are used to balance the amplitude and the delay of the two arms. Therefore, the rectangular pulse is generated in the lower arm and is subtracted from the signal in the upper arm using a balanced photodetector (BPD).

The SMF may be placed anywhere along the generator; placing it before spectral shaping avoids requiring SMF in both arms of the BPD. The length of SMF is chosen to map the pulse duration ΔT to the available source linewidth $\Delta\lambda$ via $D = \Delta T/\Delta\lambda$, where D is the total fiber dispersion.

An optical modulator (Mod_1) is used before the two-branch structure to modulate the optical pulses by the input data. In this paper, we only consider the OOK modulation scheme; however, other modulation schemes, such as pulse-position modulation (PPM), can also be implemented. The generated pulse is then amplified by a power amplifier (PA) and fed to the wideband transmit antenna via an RF circulator.

B. Receiver Structure

Amongst the various structures for the UWB receiver, incoherent structures are more attractive because they do not require information about the UWB channel; they provide low complexity and low power-consumption solutions for the detection problem [15]. It is shown that in the case of binary pulse position modulation, this strategy implements the generalized maximum likelihood test when no channel information is available [15].

In this paper, we represent a novel realization of an energy detector in the optical domain. Although the realization is more complex compared to RF incoherent realizations, many components can be reused in a half-duplex receiver, and many benefits accrue to the system. Compare, for example, the equivalent RF and optical correlator structures shown in Fig. 2(a) and (b), respectively. Ideally, the UWB pulse reference would include any distortions introduced by the wireless channel. Mixing an RF copy of the UWB pulse with the received signal and then low-pass filtering is the equivalent of imprinting the received signal onto an optical version of the UWB pulse (via external modulation) and then photodetecting. We propose that the optical signal be a simple rectangular pulse, instead of the channel-distorted UWB pulse, to reduce complexity. Also, the photodetector can

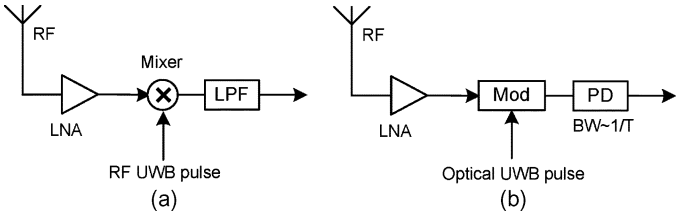

Fig. 2. Equivalent (a) RF and (b) optical correlators.

be low speed (and, thus, low cost) with response equal to the repetition rate.

As explained in Section IV-A, the transmitter generates a rectangular optical pulse with duration equal to that of the UWB pulse and with the same repetition rate. In a transceiver structure, this rectangular pulse can be used as a reference at the receiver, assuming the same transmit and receive bit rates. The received UWB signal passes first through a low noise amplifier (LNA) and then modulates an optical rectangular pulse via external modulator (Mod_2), as shown in Fig. 1. The timing between optical pulse and RF signal can be adjusted by using an optical delay line (DL_2) controlled by a synchronization signal.

The modulator is biased in order to have no output intensity when there is no RF signal. When using a Mach–Zehnder (MZ) modulator, this bias leads to full rectification, whereas an electro-absorption (EA) modulator leads to half rectification. As the modulated optical signal is immediately photodetected, full rectification gives greater detected power, and an MZ is preferred. MZ modulators are, however, sensitive to polarization. On the other hand, the electro-absorption modulators can operate on lower driving voltage with no (or less) polarization dependence and are compatible with photonic integration. Note that we do not use a CW laser, but rather an optical signal with limited duration. Thus, we impose a time window over the rectified UWB signal. For instance, a typical received UWB waveform at the MZ modulator input and the output optical signal are shown in Fig. 3(a) and (b), respectively. The signal is fully rectified and time-gated in the specified time window. Negative peaks see greater gain due to the bias point of modulator.

The received UWB pulse is longer than the transmitted pulse; the transmitted pulse is convolved with the channel response, leading to pulse elongation. To maximize the received power,

Authorized licensed use limited to: BIBLIOTHEQUE DE L'UNIVERSITE LAVAL. Downloaded on December 3, 2008 at 10:43 from IEEE Xplore. Restrictions apply.

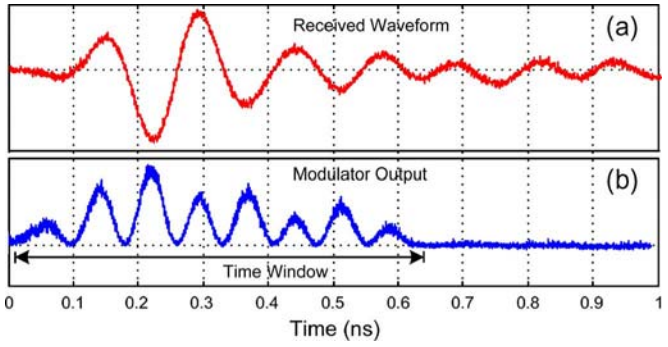

Fig. 3. (a) Typical received UWB waveform and (b) output optical signal of the MZ modulator.

the duration of the time window $\Delta T'$, or, equivalently, the duration of the rectangular reference pulse, should cover the majority of the RF received pulse. To elongate our rectangular pulse, we add another length of fiber (SMF_2) with total dispersion of D'. The fiber length is chosen to have the required time duration $\Delta T' = (D + D')\Delta\lambda$. The time windowing of the received signal is useful when we do not exploit resolvable multipath reflections; we simply truncate the tail of the received pulse. Thus, the multipath reflections have no affect on reception.

V. Experimental Results

A. EIRP Measurement

We start with EIRP measurement, using the setup shown in Fig. 4(a). Two antennas are mounted on bases and are connected to a network analyzer. For the wideband antennas, we used commercially available 3.1–10 GHz omni-directional antennas (SkyCross SMT-3TO10M-A). Two similar antennas are used for line-of-sight (LOS) transmission in a lab environment over a distance of 65 cm and a height of 120 cm off the ground. The antennas are placed in their peak radiation direction in the azimuth plane. The channel response is measured by a 20-GHz vector network analyzer (Agilent VNA-N5230A). The VNA captured 6401 points across a span of 0.2 to 14 GHz and averaged 16 times to improve the dynamic range. Observation of the channel over longer periods of time shows no differences in the response, and we conclude that the channel is non-varying.

Fig. 4(b) shows the smoothed channel frequency response. We see that the response is not completely flat in the radiation bandwidth of the antenna, and this will obviously introduce differences between the transmitted and received waveforms. Fig. 4(c) plots the channel impulse response obtained from the inverse Fourier transform of the frequency response. The inset figure shows the presence of several weak multipath reflections from the indoor environment, in addition to the main LOS response. These are mainly due to reflections from walls, ceiling, floor, and lab equipment. Use of an RF absorber placed on the ground between the two antennas reduces the multipath reflections by 75%, obviating the use of an anechoic chamber. We eliminate the remaining multipath reflections by truncating the measured impulse response.

We approximate the measured channel response, i.e, G_{CH} in Fig. 4(b), as the product of two identical antenna responses.

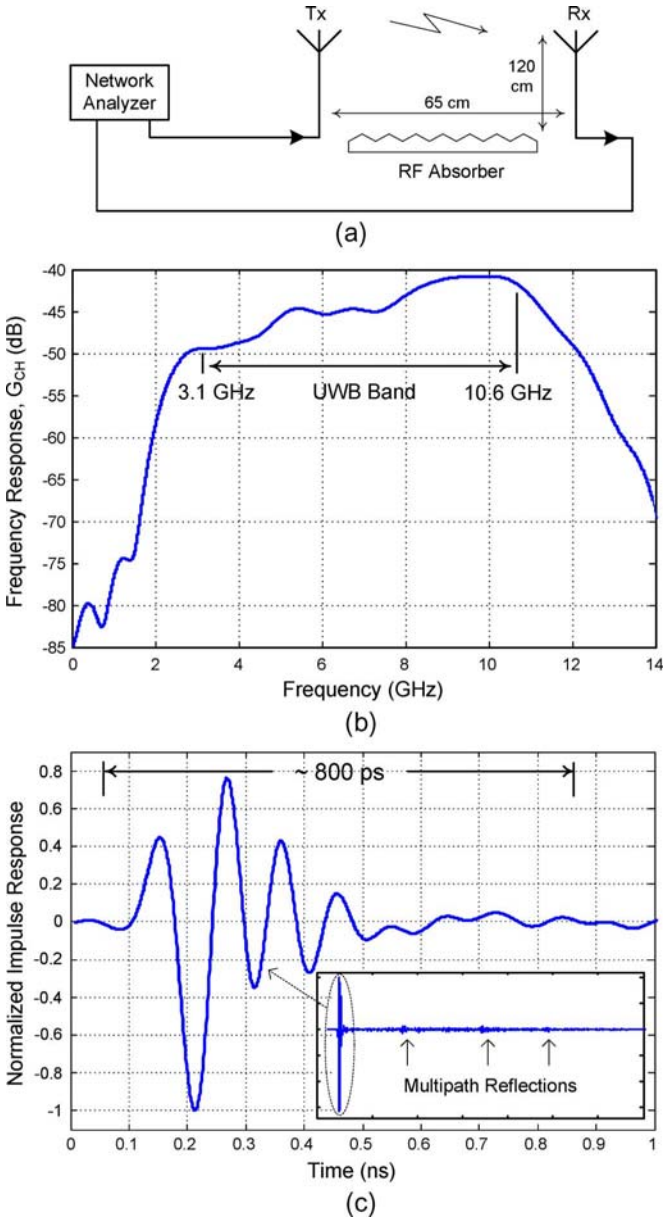

Fig. 4. Wireless LOS channel characterization. (a) Experimental setup, (b) frequency response, and (c) impulse response.

Thus, we can find the new spectral mask at the input of transmit antenna via (3); this is shown by a solid line in Fig. 5. It can be claimed that if the PSD of the UWB signal at the input of transmit antenna respects the new mask, the transmitted EIRP will respect the FCC spectral mask (dashed line).

Furthermore, in a case in which a power amplifier (PA) with an average gain of G_{PA} is used before the antenna, the modified spectral mask in (4) should be divided by G_{PA}. We used a wideband PA with a 25.7-dB gain over the bandwidth of interest (Mini-Circuits ZVA-183-S). In this case, the effective spectral mask $M(f)$ is shown by the dotted line in Fig. 5. We used this curve in our program to generate the optimized UWB waveform. It is evident that an antenna with a different frequency response would require a different spectral mask $M(f)$ and, as a result, a different optimized UWB pulse.

Authorized licensed use limited to: BIBLIOTHEQUE DE L'UNIVERSITE LAVAL. Downloaded on December 3, 2008 at 10:43 from IEEE Xplore. Restrictions apply.

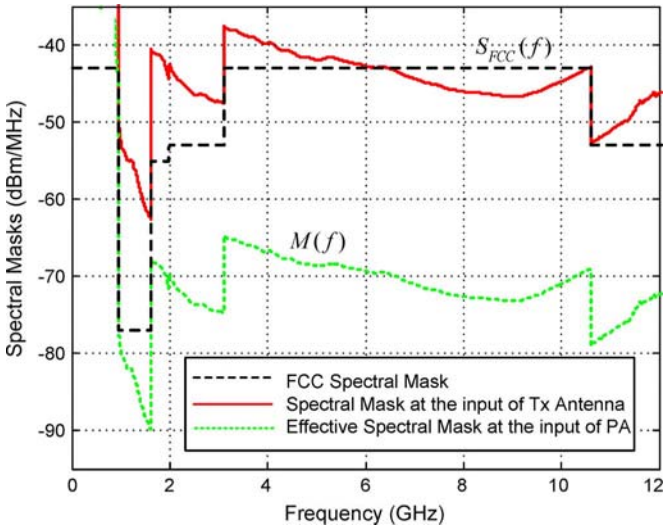

Fig. 5. FCC and the effective spectral masks.

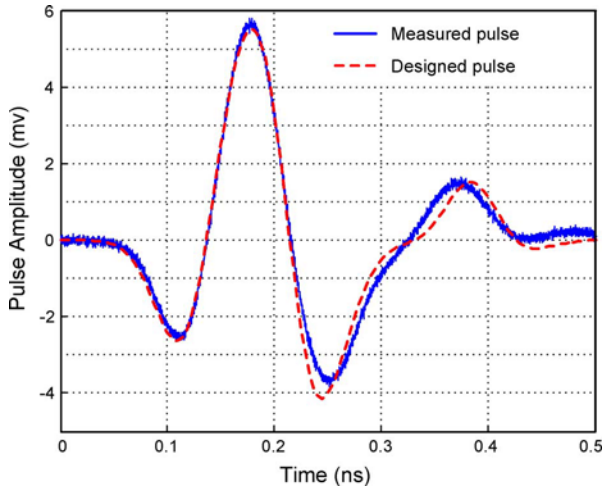

Fig. 6. (Dashed line) Designed and the (solid line) measured pulse shapes.

B. Optimized UWB Waveform

When using the dotted line in Fig. 5 as the spectral mask, the optimized UWB waveform generated by our optimization program is shown in Fig. 6 by a dashed line. We used 8 taps in (5), and T_0 and τ are 38.5 and 58.5 ps, respectively. The pulse duration is about 0.4 ns. We used 5.46 km of SMF with a measured dispersion of 16.3 ns/km/nm in order to map the 4.5-nm source bandwidth to 0.4 ns.

The generated pulse is also shown in Fig. 6, which is in good agreement with the target waveform; some deviations in the lower peak are attributable to imperfections in the FBG writing process. The PSD of both waveforms, as well as the corresponding calculated EIRPs, are shown in Fig. 7. With the appropriate choice of pulse amplitude, the PSD of the pulse is below the effective spectral mask, and as a result, the EIRP respects the FCC spectral mask.

The maximum permissible power for the input pulse is determined by the bit time $T = 1/BR$ and the modulation scheme. For $T = 2$ ns ($BR = 500$ Mb/s) and PPM modulation where a pulse is sent in each bit, the maximum peak-to-peak (p-p) voltage of the pulse is 6.8 mv, corresponding to a total power of -32.7 dBm. In the case of OOK modulation, the UWB pulse is transmitted in half of the bits (assuming equal probable input data), and the maximum p-p voltage is 9.6 mv.

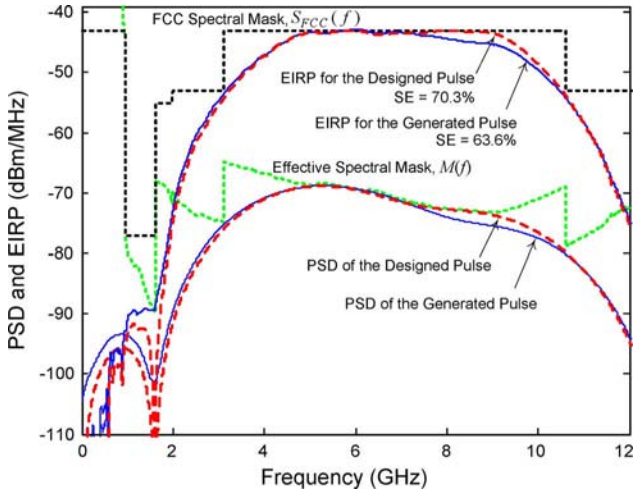

Fig. 7. PSD of the designed and generated pulse and the corresponding EIRPs.

For any p-p voltage of the pulse less than the maximum value, the PSD of the signal is completely below the effective spectral mask $M(f)$, and the EIRP respects the FCC mask. The spectral efficiency (SE) of the pulse, which is defined by

$$\text{SE} = \frac{\int_{F_p} EIRP df}{\int_{F_p} S_{FCC}(f) df}$$

and calculated over the 3.1–10.6 GHz band, is 70.3% for the designed pulse. By increasing the number of tap coefficients, greater spectral efficiencies and longer pulses can be obtained. The total average power of the generated pulse, as measured, is -32.8 dBm, and the SE of the corresponding EIRP is 63.6%.

Note that the non-optimized pulses traditionally employed in UWB applications are not able to exploit high spectral efficiency. For instance, using the same PA and transmit antenna used in this experiment, the maximum p-p voltage of the Gaussian monocycle and doublet pulses is 2.9 and 5.3 mv, with a pulse average power of -44.4 and -38.7 dBm, respectively [16]. The average power of the generated pulse here represents more than an 11.6- and a 5.9-dB improvement over Gaussian monocycle and doublet pulses, respectively.

C. BER Measurement

For 65-cm antenna separation in our prototype LOS setup, the channel impulse response in Fig. 4(c) has a duration of about 1 ns; when convolved with the input pulse, this leads to a received pulse duration of about 1.5 ns. Intersymbol interference (ISI) can be avoided at a bit rate of 500 Mb/s. Note that the transmission bit rate is only limited by ISI; the transmitter and receiver hardware and architecture can support higher bit rates. As described previously, correlation with a rectangular pulse with duration shorter than the first multipath return eliminates multipath reflections. A 5-km roll of fiber (SMF_2) at the receiver led to pulse duration extension of 0.7 ns, which permits us to retain

Authorized licensed use limited to: BIBLIOTHEQUE DE L'UNIVERSITE LAVAL. Downloaded on December 3, 2008 at 10:43 from IEEE Xplore. Restrictions apply.

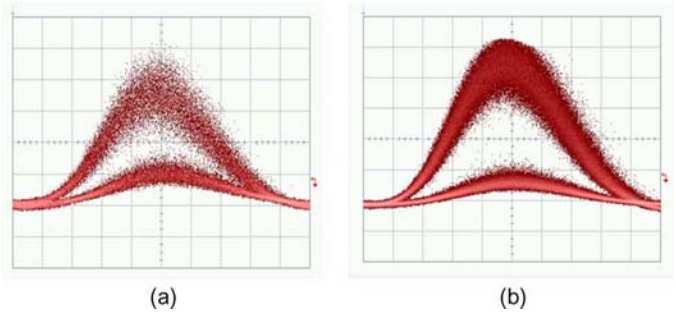

Fig. 8. Eye diagram for (a) PRBS sequence (SNR $= 3.2$, BER $= 4 \times 10^{-4}$) and (b) selected sequence (SNR $= 6.3$, BER $= 3 \times 10^{-6}$).

the main peaks of the received pulse while avoiding multipath returns.

For an optical source, we used a passive MLFL fabricated in our laboratory with a repetition rate of 31.25 MHz. To increase the repetition rate to 500 MHz, we used four MZ interferometer stages to insert 15 pulses between two consecutive input pulses [17]. Unfortunately, due to unequal losses in the directional couplers, the amplitude of the resulting optical pulses varies from one pulse to another. This has two effects: polarization that varies from pulse to pulse and an eye diagram with wide excursions on the logical ones, i.e., tending to close the eye. An active MLFL would not have this problem; unfortunately, only a passive MLFL was available to us.

While our first choice for an external modulator would be the MZ with full rectification, our source-imposed polarization independence on the modulator, i.e., an electro-absorption modulator, was used. We performed BER measurement using a 10-MHz electro-absorption modulator (Mod_2) followed by an 800-MHz photodetector. Furthermore, the BER was measured both over all pulses (as is typical), as well as over a restricted set of pulses whose height did not vary (eight of the 16 pulses).

Fig. 8(a) shows the eye diagram when a standard 2^7-1 PRBS sequence is used as OOK data. The poor eye opening is due to variations in pulse height (excursions as high as 2.5 dB). The SNR is 3.2, and the measured BER is 4×10^{-4}. The second eye diagram [see Fig. 8(b)] has data only modulating the pulses whose height is close to the nominal level; the 16 bit pattern (1110001101000011) is used. While not a PRBS sequence, it does exhibit balance and no long runs, as do PRBS, although it is a short sequence. The SNR is 6.3, and the measured BER is 3×10^{-6}. The use of a non-PRBS does not affect the generality of our results, as ISI does not play a significant role. Once again, this effect is an anomaly of the source available in the laboratory; a more stable optical source (e.g., an active MLFL) would generate an eye diagram such as that seen in Fig. 8(b).

VI. Conclusion

The limited bandwidth and the non-uniform gain of wideband antennas over the UWB frequency band has a great impact on the maximum permissible transmit power and as results on the performance of overall UWB system. In this paper, we designed a UWB waveform, taking into account the effects of the power amplifier and broadband antenna to maximize the permissible transmitted power, i.e., EIRP respects the FCC spectral mask. The measured results show that our optimized pulse has more than an 11.6- and 5.9-dB improvement over Gaussian monocycle and doublet waveforms, respectively.

Furthermore, we implemented an approximate matched filter receiver structure in the optical domain. The received RF signal modulates the existing reference optical pulse (transmitter side). This simple structure can adapt to the channel to include the time-expanded UWB pulse and yet remove the tail of the return produced by multipath reflections. The modulator acts as a full or half wave rectifier, and the integration and detection is implemented by a low-speed photodetector. In the case of OOK modulation at 500 Mb/s, the BER of 3×10^{-6} is measured for antenna separation of 65 cm. Note that no forward error correction was employed, and simple on-off keying was used. Our optical processing used hardware and an architecture that could easily accommodate higher bit rates.

Appendix

In general, SeDuMi solves problems of the form

$$\max b^T r, \tag{A1}$$

subject to $c_i - a_i^T r \geq 0$, $i = 1, 2, \cdots, n$. Transforming our optimization problem (8) to the SeDuMi format results in the following matrices:

$$\begin{aligned} \{b_i\}_{i=1}^{L} &= \beta_i \int_{F_P} |G_m(f)|^2 \cos\left(2\pi f (i-1) T_0\right) df \\ \{c_i\}_{i=1}^{N} &= M(f) / |G_m(f)|^2, \quad \{c_i\}_{i=N+1}^{2N} = 0 \\ \{a_{ij}\}_{i=1,j=1}^{i=N,j=L} &= \beta_j \cos\left(2\pi f (j-1) T_0\right) \\ \{a_{ij}\}_{i=N+1,j=1}^{i=2N,j=L} &= -\{a_{ij}\}_{i=1,j=1}^{i=N,j=L} \end{aligned} \tag{A2}$$

where N is the number of equally spaced frequency samples over the UWB bandwidth F_P. After obtaining the optimal autocorrelation vector $\vec{r}$ using the SeDuMi toolbox, we find the optimal filter tap coefficients $\vec{w}$ by spectral factorization [18].

Acknowledgment

The authors would like to thank S. Doucet and J. Magné for many worthwhile discussions and for their help with FBG design.

References

[1] S. Roy, J. R. Foerster, V. S. Somayazulu, and D. G. Leeper, "Ultrawideband radio design: The promise of high-speed, short range wireless connectivity," *Proc. IEEE*, vol. 92, no. 2, pp. 295–311, Feb. 2004.

[2] First Report and Order U.S.Fed. Commun. Comm., 2002, revision of part 15 of the Commission's rules regarding ultrawideband transmission systems.

[3] F. Zeng, Q. Wang, and J. Yao, "All-optical UWB impulse generation based on cross-phase modulation and frequency discrimination," *Elec. Lett.*, vol. 43, no. 2, pp. 119–121, Jan. 2007.

[4] C. Wang, F. Zeng, and J. Yao, "All-fiber UWB pulse generation based on spectral shaping and dispersion-induced frequency-to-time conversion," *IEEE Photon. Technol. Lett.*, vol. 19, no. 3, pp. 137–139, Feb. 2007.

[5] J. Chou, Y. Han, and B. Jalali, "Adaptive RF-photonic arbitrary waveform generator," *IEEE Photon. Technol. Lett.*, vol. 15, no. 4, pp. 581–583, Apr. 2003.

Authorized licensed use limited to: BIBLIOTHEQUE DE L'UNIVERSITE LAVAL. Downloaded on December 3, 2008 at 10:43 from IEEE Xplore. Restrictions apply.

[6] I. S. Lin, J. D. McKinney, and A. M. Weiner, "Photonic synthesis of broadband microwave arbitrary waveforms applicable to UWB communications," *IEEE Microw. Wireless Compon. Lett.*, vol. 5, no. 4, pp. 226–228, Apr. 2005.
[7] J. D. McKinney, I. S. Lin, and A. M. Weiner, "Shaping the power spectrum of ultrawideband radio frequency signals," *IEEE Trans. Microwave Theory Tech.*, vol. 54, no. 12, pp. 4247–4255, Dec. 2006.
[8] M. Abtahi, J. Magné, M. Mirshafiei, L. A. Rusch, and S. LaRochelle, "Generation of power-efficient FCC-compliant UWB waveforms using FBGs: Analysis and experiment," *IEEE J. Lightwave Tech.*, vol. 26, no. 5, pp. 628–635, Mar. 1, 2008.
[9] X. Wu, Z. Tian, T. N. Davidson, and G. B. Giannakis, "Optimal waveform design for UWB radios," *IEEE Trans. Signal Process.*, vol. 45, no. 6, pp. 2009–2021, Jun. 2006.
[10] M. Abtahi, M. Mirshafiei, J. Magné, L. A. Rusch, and S. LaRochelle, "Ultra-wideband waveform generator based on optical pulse shaping and FBG tuning," *IEEE Photon. Technol.. Lett.*, vol. 20, no. 2, pp. 135–137, Jan. 2008.
[11] D. Pozar, *Microwave Engineering*, 3rd ed. Hoboken, NJ: Wiley, 2005.
[12] F. Mlinarsky and J. Ziegler, UWB Test Report Pulse-Link Press Releases, Dec. 13, 2007 [Online]. Available: http://www.pulselink.net/press/pressreleases.htm
[13] J. D. Brunett, R. M. Ringler, and V. V. Liepa, "On measurements for EIRP compliance of UWB devices," in *Proc. IEEE Electromagn. Compat. Conf.*, Aug. 8–12, 2005, pp. 473–476.
[14] J. F. Strum, 1991, Using SeDuMi 1.02, A Matlab Toolbox for Optimization Over Symmetric Cones [Online]. Available: http://www.sedumi.mcmaster.ca
[15] C. Carbonelli and U. Mengali, "M-PPM noncoherent receivers for UWB applications," *IEEE Trans. Wireless Commun.*, vol. 5, no. 8, pp. 2285–2294, Aug. 2006.
[16] M. Mirshafiei, M. Abtahi, L. A. Rusch, and S. LaRochelle, *Wideband antenna EIRP measurements for various UWB waveforms.* ICUWB Conf., Hanover, Germany, Sep. 10–12, 2008, accepted for oral presentation.
[17] J. Magné, "Traitement optique du signal émis par un laser â fiber modelocked passif," Ph.D. dissertation, Université Laval, Quebec City, QC, Canada, Sep. 2007.
[18] S.-P. Wu, S. Boyd, and L. Vandenberghe, "FIR filter design via semidefinite programming and spectral factorization," in *Proc. 35th Conf. Decision Control*, Kobe, Japan, Dec. 1996, pp. 271–276.

Mohammad Abtahi (M'06) received the B.S. degree in electrical engineering from Shiraz University, Shiraz, Iran, in 1991 and the M.S. degree from Sharif University of Technology (SUT), Tehran, Iran, in 1994. He received the Ph.D. degree from both SUT and the Institut National Polytechnique de Grenoble (INPG), Grenoble, France, in 2000.

From February 2001 to June 2005, he has been with Iran Telecom Research Center (ITRC) as a member of technical faculty (assistant professor) and head of the Wireless Communications Group. Currently, he is with Centre d'optique, photonique, et laser (COPL), Department of Electrical and Computer Engineering, Université Laval, Quebec City, QC, Canada. His research interests are free-space optical communications, optical CDMA networks, and optical processing for ultra-wide-band systems.

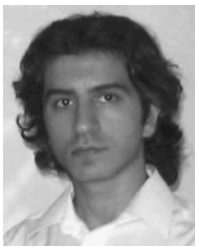

Mehrdad Mirshafiei was born on April 20, 1984. He received the B.S. degree in electrical engineering from the School of Electrical and Computer Engineering, Tehran University, Tehran, Iran. He is currently working toward the M.Sc. degree in electrical engineering with the Center of Optics and Photonics, Laval University, Quebec, QC, Canada.

His research interest is optical processing for ultrawideband pulse shaping.

Sophie LaRochelle (M'00) received the Bachelor's degree in engineering physics from Université Laval, Quebec City, QC, Canada, in 1987 and the Ph.D. degree in optics from the University of Arizona, Tucson, in 1992.

From 1992 to 1996, she was a Research Scientist with the Defense Research and Development Canada-Valcartier, where she worked on electro-optical systems. She is now a professor with the Department of Electrical and Computer Engineering, Université Laval, where she holds the Canada Research Chair of Optical Fibre Communications and Components. Her current research activities are focused on active and passive fiber-optics components for optical communication systems, including fiber Bragg gratings, optical amplifiers, ans multi-wavelength and pulsed fiber lasers. Other research interests include packet-switched networks with photonic code processing, transmission of radio-over-fiber signals, and OCDMA.

Dr. LaRochelle is a member of OSA and of IEEE-LEOS.

Leslie A. Rusch (S'91-M'94-SM'00) received the B.S.E.E. (honors) degree from the California Institute of Technology, Pasadena, in 1980 and the M.A. and Ph.D. degrees in electrical engineering from Princeton University, Princeton, NJ, in 1992 and 1994, respectively.

She was previously the manager of a group researching new wireless technologies at Intel Corp. from 2001 to 2002. She is currently a Full Professor with the Department of Electrical and Computer Engineering, Université Laval, Québec, QC, Canada, performing research on wireless and optical communications. Her research interests include optical-code-division multiple access and spectrum-sliced WDM using incoherent sources for passive optical networks; semiconductor and erbium-doped optical amplifiers and their dynamics; radio over fiber; wireless communications; and high-performance, reduced-complexity receivers for ultra-wide-band systems employing optical processing.

Authorized licensed use limited to: BIBLIOTHEQUE DE L'UNIVERSITE LAVAL. Downloaded on December 3, 2008 at 10:43 from IEEE Xplore. Restrictions apply.